

# Investigation of characteristic rippling topology produced during UHMWPE sliding

K.G. Plumlee<sup>1</sup> and C.J. Schwartz<sup>2,\*</sup>

<sup>1</sup>Dept. of Mechanical Engineering, Oklahoma Christian University, Oklahoma City, OK, USA

<sup>2</sup>Department of Mechanical Engineering, Iowa State University, Ames, Iowa, USA

## Abstract

Ultra-high molecular weight polyethylene (UHMWPE) remains the sole polymer bearing material for use in orthopedic implants and its behavior has been studied extensively. Various techniques, such as crosslinking, have been employed to reduce the total wear volume. However, little is known about the actual wear mechanisms that contribute to the removal of debris from the bulk. A nearly universal observation of the wear surfaces after multidirectional sliding of UHMWPE is the presence of regularly-spaced parallel ripples whose wavelength closely matches debris size. In spite of the fact that this phenomenon has been observed for decades in both retrieved implants as well as wear simulation studies, the specific causes of the rippled topology have not yet been identified. Proposed mechanisms have included abrasion, crystallinity effects, fatigue, stick-slip behavior, thermal softening, and Schallamach waves. This investigation involved an experimental and computational factorial test design to determine the role of various parameters involved in the rippling phenomenon. The authors employed a film buckling theoretical model and applied it to UHMWPE using a finite element modeling approach. Wear testing was performed on a two-axis tribometer to expose the polymer to multi-directional sliding. Characteristic ripples developed on all wear surfaces, but with varying periodicity. Two regimes of the ripple phenomenon were observed: localized long wavelength (2.2 – 3.2 micron) ripples which appeared to dominate before steady state wear was established, and long-range shorter-wavelength (approximately 1 micron) ripples which indicated a steady-state condition. Surprisingly, feature wavelength showed little dependence on roughness or temperature but were slightly affected by contact pressure. The wear surfaces were cleaved and examined by SEM to gauge the thickness of the plastically deformed quasi-film layer. These layers were on the order of 10 to 20 nanometers thick. Further examination of the surfaces confirms the development of a deformed layer which acts similarly to a buckled thin film.

## 1. Introduction

Ultra-high molecular weight polyethylene (UHMWPE) remains the most popular bearing material for use in artificial joints. As a result, the wear of UHMWPE has been studied extensively, mostly focused on the negative effect of wear debris on the body [1], and various techniques to reduce the total wear volume, such as crosslinking [2]–[7], and composite fillers [8]–[14]. Despite the quantity of studies, investigators continue to seek a stronger understanding of the actual wear mechanisms that contribute to the removal of debris from the bulk. Looking for insight into wear mechanisms, observation of the resultant wear surfaces reveals a polymer surface generally free

of cracking and deep abrasive scratches, but does typically exhibit a periodic, rippled geometry whose wavelength closely matches debris size, with evidence that debris is removed from the peaks of each ripple. This geometry has been observed in many studies on retrieved implants [15], [16] and wear simulators [13], [16]–[19]. Dowling and Charnley commented on the phenomenon in the late 1970s, stating “the cause of the parallel ripples has not yet been identified” [15]. Since then, multiple mechanisms have been proposed for the formation of these ripples, including abrasion [20], crystallinity effects [13], [17], [21], fatigue [22][23], stick-slip behavior [24][25], thermal softening [26] [27], and Schallamach waves [28], [29]. While the root cause may not be known, it is generally accepted that most bioactive debris particles originate from the peaks of these ripples, and that plastic deformation of the surface plays a role. In 1995, Wang, Stark, and Dumbleton reached similar conclusions, stating “It is still not well understood how the ripples are formed...but it is generally accepted that accumulated plastic deformation plays a critical role in the formation of the ripple-like features on the surface of the acetabular cups [30].” Previous studies have shown experimental evidence of shear strain 5-10  $\mu\text{m}$  below the surface [31], and shown that crystalline lamella within the polymer orient along the direction of plastic deformation up to a depth of at least 4-10  $\mu\text{m}$  [32].

One possible explanation for the ripples sprouts from the idea that the aforementioned plastic deformation occurs at the surface without that material being detached from the bulk [31], [32], resulting in a strained surface layer that eventually buckles as the stress relaxes. This is essentially a film that is produced with profoundly different strain history than the bulk. If the strained surface layer is uniform in thickness, the buckled film would form a periodic pattern perpendicular to the principle stress direction [18], [33]. Similar results have been seen in thin-film depositions of polymers onto metals [34]. In the model proposed by Stafford *et al.*, which is based on a strain energy equilibrium of film layers, the elastic moduli of the bulk and film are included but it is the thickness of the film itself which plays the largest role in determining the wavelength of the ripples resulting from buckling [33]. It is not evident from the literature that this model has been employed previously in the investigation of the UHMWPE rippling phenomena.

The depth of the plastically deformed layer of worn UHMWPE is the hypothesized effective film thickness in a buckling mechanism. The current standard for predicting the onset of plastic deformation in polymers is the Von Mises yield criterion, also known as the  $J_2$ -plasticity theory. This theory is often applied to ductile materials, and is particularly common in computer modeling. Unfortunately, there is evidence that Von Mises stress is not ideal for use in UHMWPE wear [35]. Additionally, the size scale of wear phenomena ( $< 1 \mu\text{m}$ ) are on the border of necessitating the inclusion of additional molecular factors, such as individual chain alignment, semi-crystalline regions, and intermolecular forces; all of which may lead to anisotropy within the material. These effects are not typically included in Von Mises yield criterion or continuum mechanics (and subsequently, finite element analysis), and therefore may not accurately predict the formation of surface films or ripples.

This study aimed to better understand which parameters have an impact on the rippled surface phenomenon of worn UHMWPE, and to determine the extent to which standard wear simulation

parameters impact the prevalence and size of these surface features. This investigation involved an experimental study of the resulting rippling behavior produced by changes in three sliding parameters – namely pressure, temperature and counterface surface roughness. The work also employed a computational approach to simulate stress and strain conditions at the interface, to provide additional insights into the results of the experimental study. In addition to exploring the connection between the traditional von Mises based methods of predicting yield and the observed surface rippling, a final goal was to get direct observation of the plastically deformed layer developed within only a few sliding cycles.

## **2. Materials and Methods**

### *2.1 Experimental Investigation*

Experimental wear tests were performed to explore the range and consistency of the rippled surface topology with respect to three sliding parameters: 1) apparent contact pressure, 2) counterface temperature, and 3) counterface surface roughness. Later in the study, as described below, a computational study focused on these same parameters. While the wear of UHMWPE is of utmost importance in biomedical applications, the specific goal of this study was to understand the topological phenomena *induced* by wear, rather than the absolute extent of material removal. These experiments were performed using GUR-4150 UHMWPE (Ticona), which was compression molded into 6.25-mm diameter cylinders with a length of 18 mm. The goal of this study was not to necessarily replicate in vivo conditions, but to employ materials and methods that would give insight into fundamental mechanisms and trends. Thus the polymer material was not crosslinked via irradiation or other means as would be expected in an implanted acetabular cup. Tests were conducted on a custom built tribometer (Fig. 1), which provides two axes of motion, and uses variable pneumatic cylinders to apply contact pressure between the samples and the counterfaces. As shown in the figure, up to four UHMWPE pins can be affixed to individual pneumatic cylinders, which are attached to the upper plate. The cylinder support plate reciprocates along one axis via an electric gear motor and crank. The lower plate holds corresponding individual counterfaces, and is driven in a perpendicular direction, resulting in a circular wear path between counterface and UHMWPE pins. An electric heater is affixed to the bottom of the lower plate to control the temperature of the counterfaces. Counterfaces consisted of 90mm square plates made from stainless steel (type 410, 45 HRC), which were polished to two different degrees of roughness values:  $R_a = 0.005 \mu\text{m}$  and  $0.030 \mu\text{m}$ . Because of the strong impact of multi-directional sliding on the wear of UHMWPE, this investigation exposed the wear interface to sliding with considerable cross motion. The polymer specimens traced out 50 mm diameter circles at a sliding speed of approximately 180 mm/s for a total sliding distance of approximately 42.5 kilometers. (approximately 250,000 cycles). While the sliding speed is higher than for standard simulations of orthopedic conditions, it was shown that very similar surface topologies were produced with the sliding speed used in this study. Before testing, the wear surfaces of the polymer pins were gently finished against a fine grit abrasive paper to ensure planar contact with the counterface, but roughness metrics were not obtained. Examination of untested pins and unworn sections of tested pins indicated that the as-finished surfaced did not have undulations.

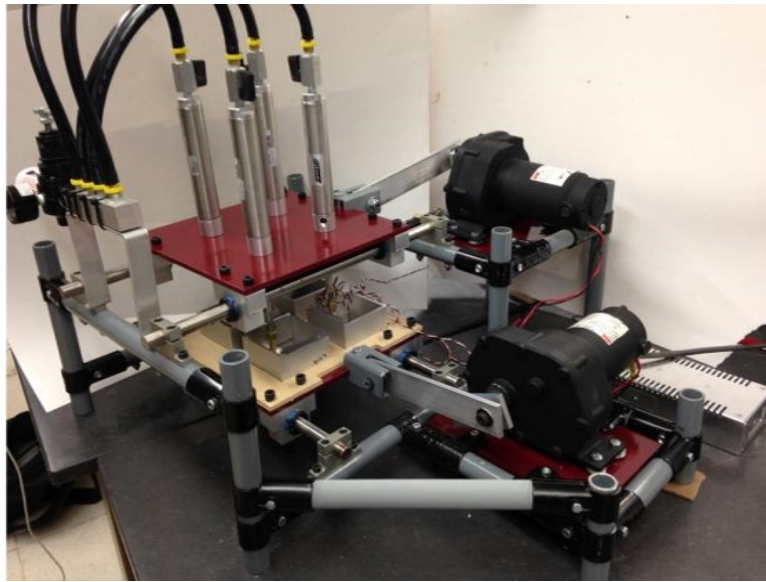


**Figure 1: Illustration of the custom built two-axis tribometer used in this study. The pins are held in fixtures attached to the pneumatic cylinders while the steel counterfaces are mounted below.**

Wear tests were performed under dry sliding at apparent contact pressures (i.e. normal force divided by the surface area of the wear interface of the pin) of 2 MPa and 6 MPa to balance the size and torque constraints of the test apparatus. These pressures were also used in the computational modeling. Rather than perform tests specifically at *in vivo* temperatures (37°C), the investigators sought to observe the impact of temperature on behavior at two levels which were below and above *in vivo* conditions, respectively. The temperature of the counterface was regulated to either 28° C or 50° C ( $\pm 1^\circ$  C) through a heat strip applied to the back of the counterface, and controlled via temperature controller and thermocouple, and verified with an infrared thermometer. Each test setting was repeated twice to confirm the consistency and repeatability of each test setting.

Previous investigations have yielded ‘wrinkled’ or ‘rippled’ UHWMPE wear surfaces which can be either localized or widespread across the worn interface [26], [30]. These features typically have a spatial period, termed *wavelength* for the remainder of this paper, which ranges from 0.5 to 5  $\mu\text{m}$ , with ridge heights less than 1  $\mu\text{m}$ . The general shape is loosely sinusoidal, although the peaks are often flattened or drawn out into fingers, suggesting that small debris particles are liberated from these asperities. At the conclusion of each wear test, the resultant wear surface was imaged using a scanning electron microscope (NEON 40 EsB, Carl Zeiss Microscopy Ltd., Cambridge, Massachusetts, USA), with a specific focus on ripple topology. Ripple wavelength from these images was characterized using image processing software (ImageJ software *version 1.8.0*, National Institutes of Health, Bethesda, MA, USA). To get a representative sampling of wavelength of the entire wear surface of a pin, measurements were taken by averaging the length across multiple ripple peaks, and this process was performed multiple times across each SEM image. Each sample was imaged multiple times across the surface, and each image covered a width of approximately 30-50 wavelengths to maintain adequate resolution. Ripples were observed in all

test specimens to varying degrees, and wavelengths were recorded from multiple locations across a sample face, with a minimum of ten measurements for each sample.

It was a hypothesis of the investigators that a previously developed thin-film buckling model (described in the next section) may be a useful tool for understanding ripple formation and characteristics. The investigators compared the experimentally generated wear surfaces to this model. However, additional work was done to validate the presence of a plastically deformed layer (or film) being generated at the wear interface of UHMWPE. A novel method was employed to experimentally observe the thickness of the deformation layer, which also allowed for observing topological changes over a few wear cycles. To accomplish this, additional wear samples were generated by wearing specimens according to the same test parameters as above, then cutting a thin groove on the wear surface by lightly scratching across the center with a fresh razor blade. This produced a clean and shallow groove in the wear surface, approximately 10  $\mu\text{m}$  across and a depth of approximately 5  $\mu\text{m}$ . Grooved samples were then placed back in the tribometer and worn for a small number of additional cycles, followed by SEM examination. This provided additional insight into the distribution of plastic deformation and the thickness of the deformed layer.

## 2.2 Thin Film Buckling Model

As stated above, the investigators hypothesized that UHMWPE rippling might be an example of buckling of a thin deformed layer which forms on the wear interface due to the stresses and temperatures produced during sliding. The fundamental topological parameter – ripple wavelength,  $\lambda$  – is a result of the coordinated buckling and stretching of the film and substrate, described in the following equation from Stafford et al.,

$$\lambda = 2\pi h_f \left( \frac{E_f / (1 - \nu_f^2)}{3E_s / (1 - \nu_s^2)} \right)^{\frac{1}{3}} \quad (1)$$

Where  $E$  is elastic modulus,  $h_f$  is the thickness of the film, and  $\nu$  is Poisson's ratio. Subscripts of  $f$  and  $s$  refer to the film layer and the substrate, respectively. It was assumed that the elastic properties of the bulk and deformed UHMWPE were reasonably similar, though they were not directly measured. This assumption, if true, greatly simplifies the interpretation of the above model with respect to the most dominant parameter controlling wavelength by reducing wavelength to be proportional to film thickness with a coefficient of approximately  $1.39\pi$ . The film thickness would presumably be determined by the depth of plastic deformation experienced by the polymer during sliding. This implies that wear parameters related to polymer yielding would also affect the ripple wavelength, thereby providing useful avenues for exploring the mechanism. Numerous images of UHMWPE ripples both from the literature and previous work by the authors reveal a typical ripple wavelength – and thus a predicted depth of plastic deformation – on the order of microns [2], [13],[15],[22]. The grooved wear pins, described above, as well as the computational modelling, described in the next section, were used to ascertain whether there was any evidence to support this prediction of film thickness based on wavelength.

### 2.3 Computational Modeling

To obtain a first-order approximation of behavior to complement the experimental findings, finite element analysis (FEA) was performed using a commercial software package (ANSYS 18.0 Structural Analysis). To replicate the topology of the wear surface of the physical samples, surface profile data was collected from worn samples via atomic force microscopy (Asylum MFP-3D), and non-contact, white light profilometry (NewView 600s, Zygo Corp., Middlefield, Connecticut, USA). This data was imported into the finite element model as four-node, 2-D plane strain elements, and was selected to ensure that both bodies had multiple asperities represented. Tensile stress-strain behavior for GUR-4150 employing the ISO-527 standard was provided by the polymer supplier (GUR 4150, Ticona), and was imported into the model as a multi-linear kinematic hardening curve, as shown in Figure 2. The bulk physical properties applied for stainless steel and UHMWPE are shown in Table 1. A representative friction coefficient of 0.1 for UHMWPE on stainless steel was applied within the software.

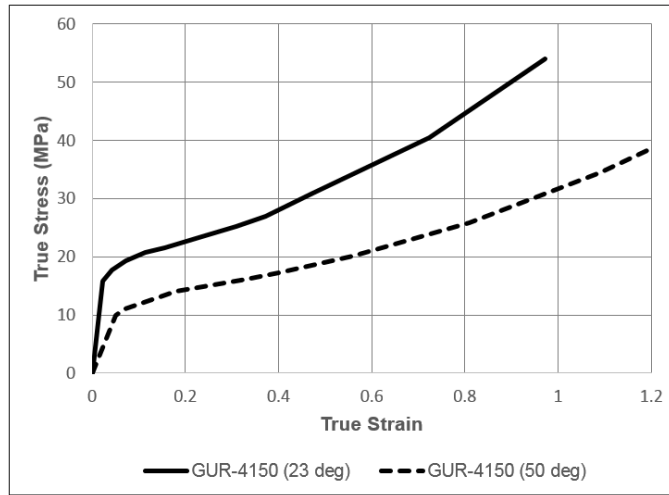


Figure 2: UHMWPE properties used in FEA, at 28° C (solid), and 50° C (dashed).

Table 1: Physical properties of materials used in FEA.

	Density (kg/m <sup>3</sup> )	Modulus (GPa)	Poisson's Ratio
Stainless Steel	7750	193	0.31
GUR-4150 (23° C)	930	0.68	0.4
GUR-4150 (50° C)	930	0.2	0.4

Appropriate boundary conditions were used in the modeling as follows. The base of the UHMWPE body was fixed, and mirror boundaries were applied to the sides. The comparatively short counterface body was positioned above the UHMWPE body to ensure the part would remaining fully supported, then a pressure (2 or 6 MPa) was applied to the back of the counterface,

forcing the two components together, as shown in Figure 3. Load levels were chosen to fall within the range of expected loads for artificial hips of less than 10 MPa [36], while allowing for ease of experimental testing later in the study. A node-to-surface contact algorithm was employed for this study. Once the bodies had come into initial contact during the simulation, the counterface was laterally displaced by a distance of 5  $\mu\text{m}$  while still under load. Meshing was refined using an automatic convergence tool within ANSYS, which refined the mesh near high stress areas until the regions changed by less than 3% with each subsequent step. The final mesh had elements near the surface that were relatively equiaxial, approximately 75nm across, but elements got larger as they were further from the contact points. Maximum von Mises stress and maximum plastic strain levels were recorded during the simulation. To estimate the thickness of the deformed layer (with regards to the buckling model), the maximum perpendicular distance from the contact surface to a sub-surface location where the plastic deformation exceeded 0.001 strain was recorded.

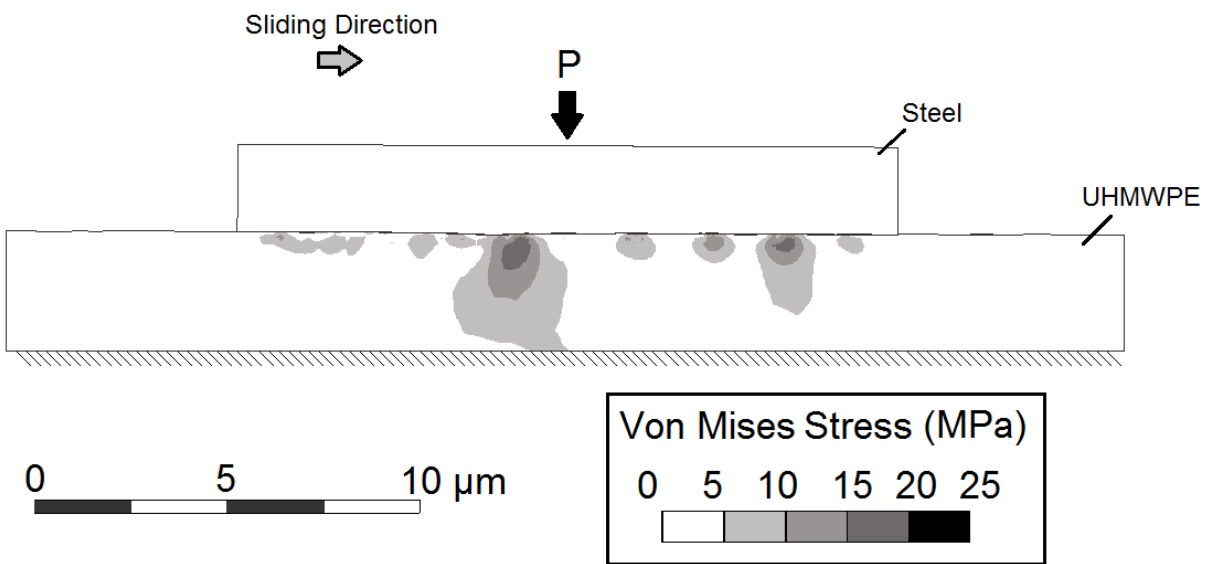


Figure 3: Example finite element model using imported surface geometries and contact pressure,  $P$ , of 6 MPa. Von Mises stresses are shown for UHMWPE body, on lower portion.

### 3. Results and Discussion

#### 3.1 Experimental Results

##### 3.1.1 Wear tests

The general appearance of the surfaces was comparable to the results of the previous work cited with regards to ripple topology. For instance, such characteristics were reported in explanted acetabular cups by McNie, et al. [22], and in explanted tibial inserts by Wimmer, et al. [37]. Intriguingly, the orientation of such ripples has been shown to vary between hip and knee arthroplasties. The ripple formations could be easily classified into two main types based on extent of coverage: fully-developed, which covered large areas, and under-developed, which covered

much smaller areas. These two groups were also easily distinguished by wavelength, as seen in Figure 4.

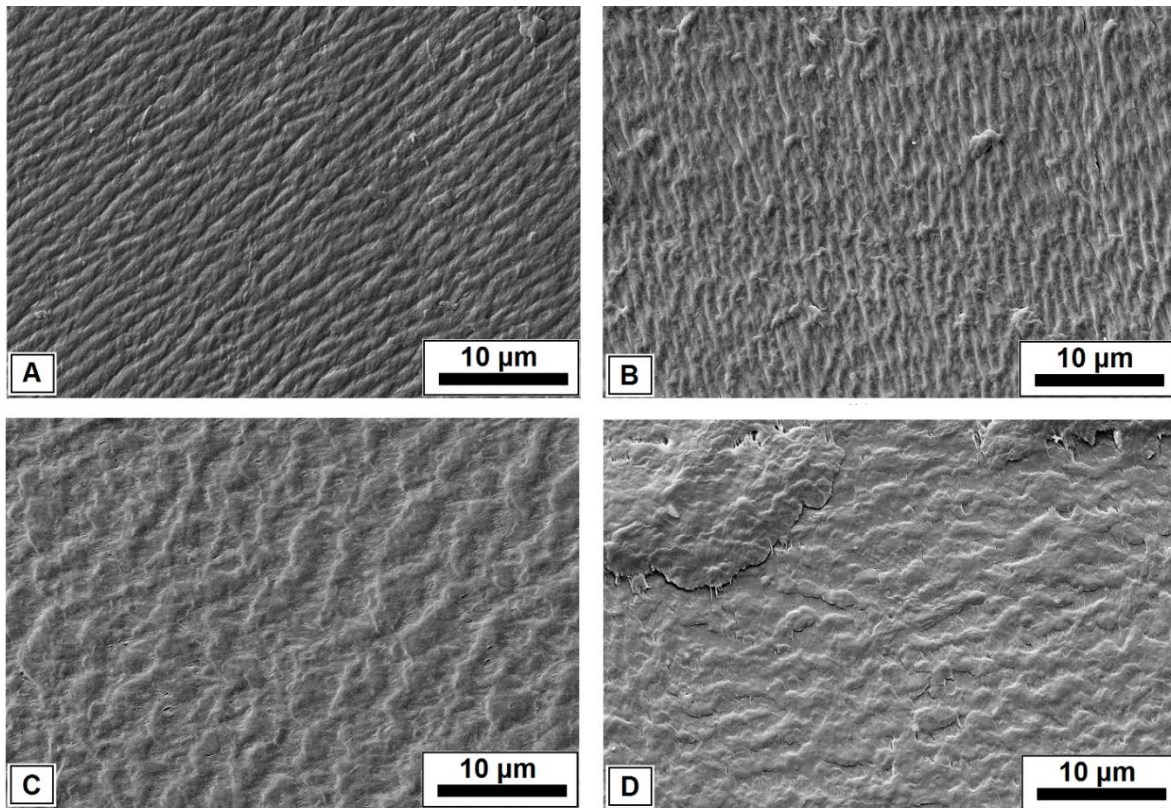


**Figure 4: Rippled topology produced by wear testing at 28° C, at (A) 2 MPa pressure, and (B) 6 MPa pressure. (C) and (D) illustrate longer wavelength rippled regions in samples produced under 2 MPa pressure, but at 50° C.**

While the presence of the ripple phenomena was observed in all tested samples, there was a large variation in wavelengths and areas of coverage. This variation between samples suggests that the formation of ripples was more dynamic than initially predicted. Two possible explanations are presented here: 1) A widespread and uniform rippled surface is a steady-state phenomenon, but the difference in test settings required different durations to achieve steady state, and therefore produced different levels of development; or 2) the rippled areas are not a steady feature, but instead progress through a cycle of development, wear down, and regeneration as material is removed from the bulk. Figure 5 reports the measured wavelengths for the ripple features produced in each of the test combinations, as well as whether both topologies (fully developed vs. underdeveloped) were observed. The figure is divided into the low temperature test runs on the left separated from the high temperature tests on the right. One of the seven experimental configurations is not reported because the measurements were discovered to be unusable due to experimental error.

The results for the low temperature tests appeared to be more consistent than the high temperature testing in terms of initial expectations about wear interface behaviors. Overall, the initial observation that can be made is that there is a clear difference between the mean wavelength

of what is referred to as an ‘underdeveloped’ ripple topology, and that of ‘fully developed’ ripple topology, with the former have a wavelength which were two to three times higher than the fully developed features. What is less clear, however, is which of the individual sliding parameters (pressure, temperature, and surface roughness) have a direct impact on wavelength, if any. To further explore the impact of the factors, a three-way analysis of variance (ANOVA) was performed to search for main effects as well as interactions. The analysis revealed the distinction between fully developed and under developed ripples has a potential correlation to the interaction between temperature and pressure ( $p = 0.08$ ), though this is not with extremely strong credibility. It has been previously shown that the coefficient of friction of many polymers changes with temperature, as does wear rate [38]. The potential interaction may be an indirect reflection of this behavior. Surprisingly, none of the other factors, nor their interactions, showed strong evidence of a direct impact on ripple wavelength, based on statistical significance at the 0.05 level. As stated above, though certain test parameters consistently resulted in fully developed ripples, most settings resulted in a combination of both types of ripples, suggesting that ripple formation is a dynamic process. One possible explanation for this observation is that these two different surface topologies are due to differences in the evolution of the wear surface. To maintain consistency in this study, every sample was worn for the same duration of time; however, not every sample had the same mass loss rate. It is expected that the fully developed ripples were more representative of samples that achieved near steady state conditions, and are therefore better matched to the finite element modeling. Underdeveloped samples have less consistent surfaces, and are likely the result of not yet achieving steady conditions.

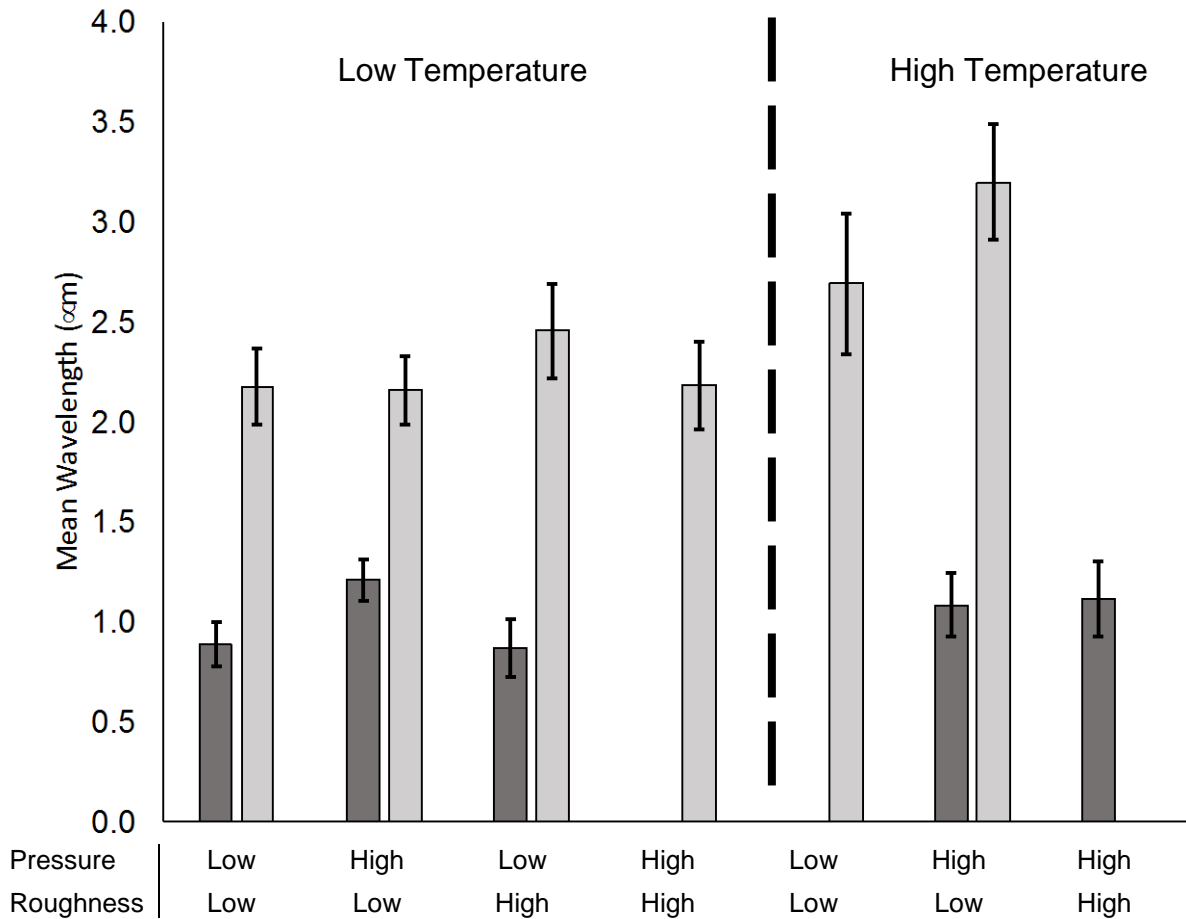


**Figure 5: Overview of ripple wavelength across multiple samples based on test setting, with error bars showing one standard deviation. Ripples were categorized into two distinct groups: fully developed ripples (dark grey) covered regions hundreds of wavelengths wide, while underdeveloped ripples (light grey) were less consistent and covered small areas. Sample size of each treatment was  $n = 2$ .**

Fully developed ripples were found in nearly every combination of test parameters, and remained consistent from sample to sample, with the mean wavelengths ranging from 0.8 to 1.2  $\mu\text{m}$  across all samples. These regions covered significant portions of the wear surface, extending many hundreds of microns or more, even up to the edge of the sample, as shown in Figure 6. Though analysis did not reveal any statistically significant correlations between wavelength and any test parameters (pressure, temperature, or roughness), the strongest potential effect was contact pressure ( $p = 0.21$ ). While this does not provide strong evidence to reject the null hypothesis (no pressure effect), it is intriguing that the finite element results presented below suggested pressure should be strongly correlated to film thickness and thus ripple wavelength. It is conceivable that a larger number of samples might better elucidate whether pressure does play such a role.

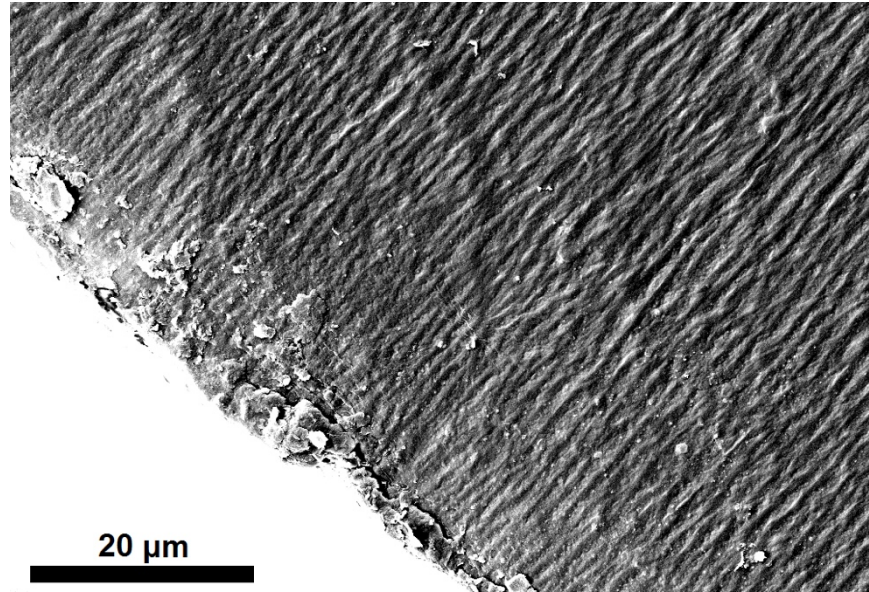


**Figure 6: Ripples extend almost completely to edge of sample, without noticeable change in wavelength.**

Additional observations from the fully developed regions include changes in directionality of the ripples. On a local scale of a few hundred microns, the ripples appear to maintain a relatively uniform direction and consistent spacing, but across the full span of the sample, the direction of the ripples changes (Fig. 7) and the wavelength may vary by up to 40%. This change in direction is most likely a result of the preferential stress directions that arises due to the flexure of the sample during the wear tests. As the sample moves in a circular pattern, the sample bends slightly due to friction, creating an uneven load profile across the surface. This has two implications: 1) the samples are not experiencing symmetric, two-axis motion, thus shear-induced orientation of the polymer chains might be along different directions at different locations on the wear surface, and 2) the actual contact pressures experienced by the sample in localized areas may be significantly greater than the expected values.

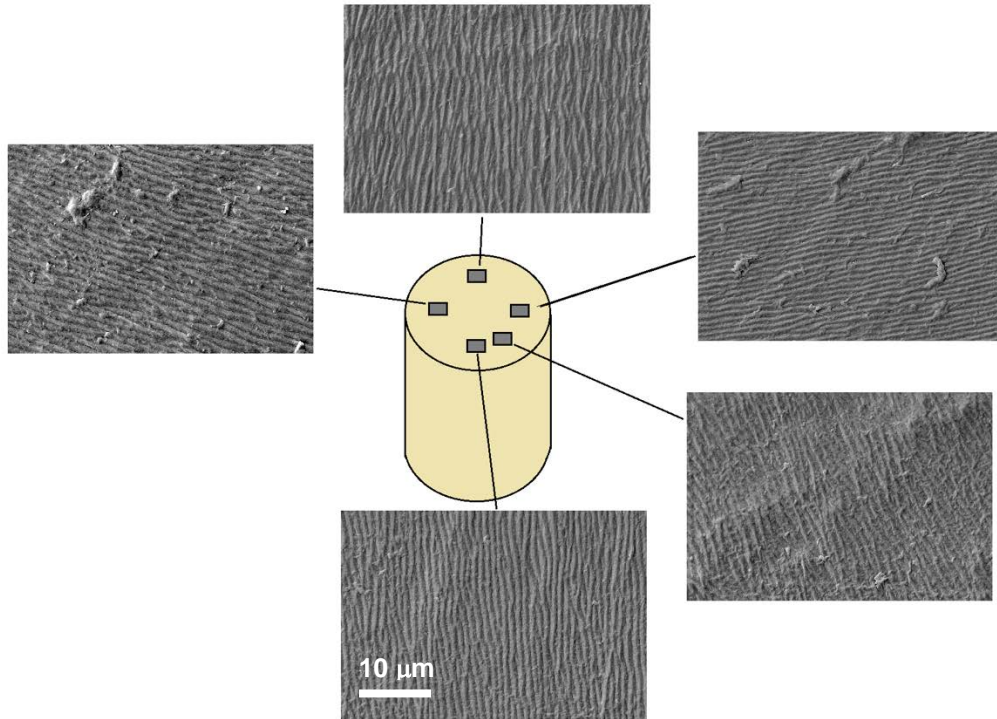


**Figure 7: The orientation of the ripples varied depending on the location around the perimeter of the wear surface, likely due to the flexure of the sample under frictional load. Scale bar indicates the identical magnification of all micrographs.**

In contrast to the fully developed regions of ripple topology, the under-developed ripples had much smaller regions of coverage, and the individual patterns were far less defined and consistent. Additionally, the wavelength was between two and three times as large as the fully developed ripples, ranging from 2.15-3.15  $\mu\text{m}$  in wavelength. Inspection of the data suggests the spacing associated with this phenomenon may have a mild dependence on temperature. It is suspected this phenomenon is associated with wear processes that are approaching, but have not quite achieved, steady state conditions. During these transient periods of wear evolution, contact stresses would be less uniform, and layers of deformed material would be present but less consistent, resulting in loose semi-rippled geometry. As the samples continued to wear, the strained layer becomes more widespread, thinner, and crisper in detail, giving smaller ripples. Supporting this possible explanation, Barrett *et al.*, demonstrated that both the wear rate and friction coefficient of UHMWPE on stainless steel are dynamic, particularly between 50° C and 66° C [38], noting that larger debris flakes form in higher temperatures, which disrupt the wear surface. This dynamism would result in poor film generation, and would help explain the relationship between wavelength and temperature – cooler temperatures experience more steady wear, and therefore more consistent ripples. It is possible that the conditions would eventually stabilize, in which case, ripple wavelength would only be dependent on temperature early in the wear process, but would become less influenced by temperature as steady state conditions are reached. This would match the results of computer models, since the simulations were performed using steady state surface geometries

and conditions. Tests of long duration and/or sliding distance would likely need to be performed to verify this hypothesis.

### 3.1.2 Grooved-Surface Testing

While no strong correlations between the testing parameters and ripple wavelength were observed based on the wear testing results, attention was turned to the results of the low-cycle wear testing with grooved surfaces to better understand the surface deformation process. Freshly grooved samples that experienced no additional wear were observed to have clean groove edges in SEM images, whereas grooved samples that had additional wear cycles exhibited noticeable changes to the groove geometry (Fig. 8). These changes occurred in as little as a single wear cycle, and are observed across the entire surface of the sample, suggesting that large-scale plastic deformations does indeed occur. Occasional flake-like debris, typically associated with adhesive wear, were also seen bridging the groove, potentially acting as a self-adhering mobile solid lubricant film as these particles migrated across the wear surface.

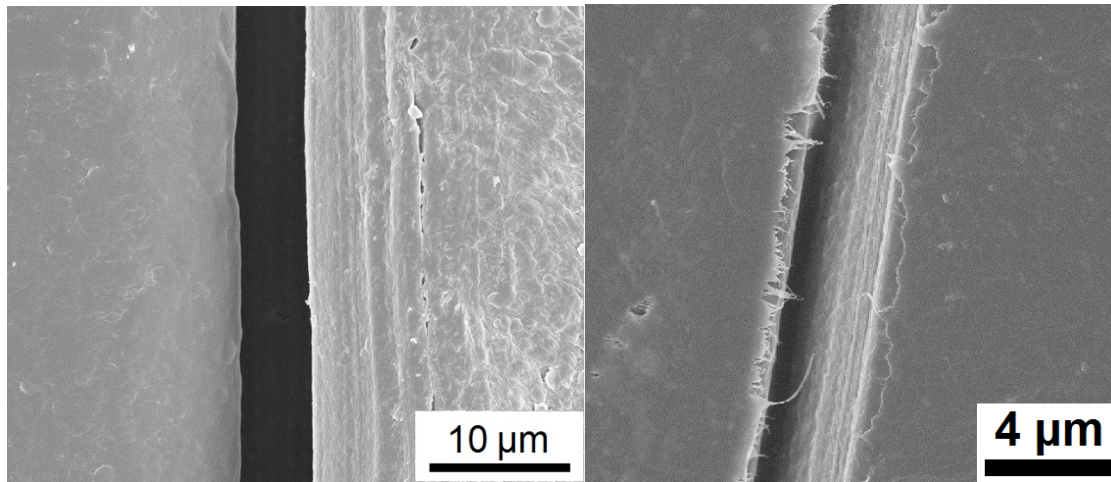
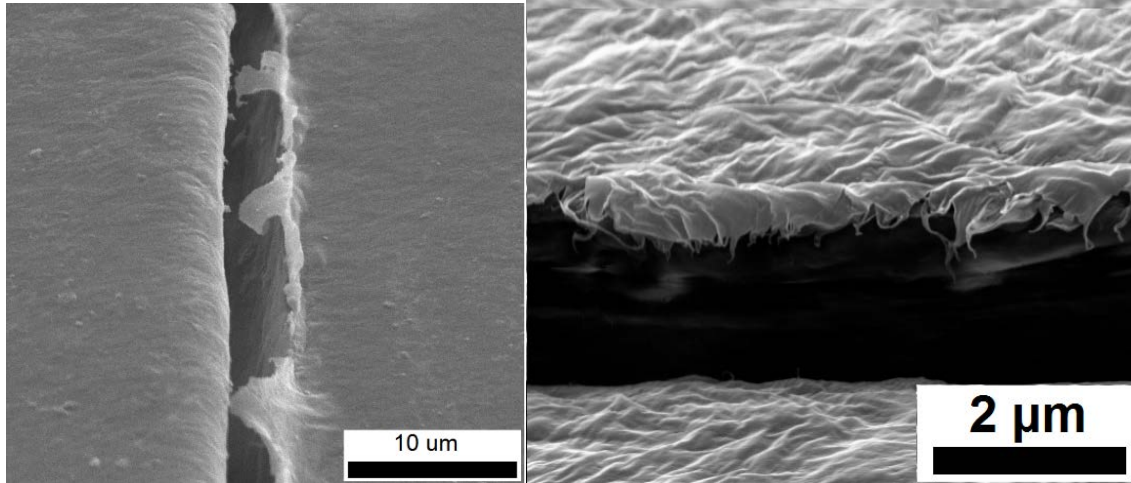


Figure 8: Pristine groove with no additional wear cycles (left). Groove after 3 cycles of motion at 2 MPa against the smoothest counterface (right).

The typical formations seen near the groove boundary include thin sheets and fingers that appear to be substantially less than 1 micron in thickness. This is significantly thinner than what is predicted by the computation modelling, described in the next section. Additionally, the finite element models suggested a smooth gradient of deformation penetrating into the bulk surface layer up to 1  $\mu\text{m}$ , whereas the groove test results show the thin film is reasonably discontinuous from the bulk surface (Fig. 9). These thin sheet formations occurred in every sample setting, and no difference in film thickness or coverage was observed. Better measurements may reveal more insight into these deformation mechanisms, however, when higher magnification images were attempted in the SEM, the extremely thin polymer sections experienced melting and warping. The high level of deformation sustained by this layer in a single motion suggests this zone behaves much like a disconnected film. It may even be possible that it functions as a localized solid lubricant allowing low friction and relative motion between the bulk polymer and the substrate. A possible explanation for this behavior is that this transfer layer is created from a buildup of polymer

that has already been liberated from the bulk. While the scale of this deformed layer is much less than what was hypothesized by the buckled film model, these results confirm that at least some amount of surface topology is a result of a thin deformed film acting somewhat independently of the bulk polymer substrate. It must be noted that these conclusions are made with the assumption that the elastic properties of the bulk and deformed UHMWPE were reasonably similar as stated above.



**Figure 9: Worn grooves viewed from 60° angle. In contrast to finite element models, there is no sign of a gradient of deformation penetrating up to 1  $\mu\text{m}$  into the surface, rather, a thin surface layer with drawn fingers, approximately 10-20nm in thickness is observed.**

### 3.2 Computational Modeling

Each experimental setting used in the computational modeling was replicated to yield a sample size of two tests for each configuration. Using maximum depth of plastic deformation as a response variable, ANOVA was performed on the FEA results to determine the role of the various factors and interactions. The results suggested that contact pressure had the strongest influence on plastic deformation of the three parameters studied. This is intuitive, but like the experimental results, there was not extremely strong statistical evidence of such with a p-value (0.09) falling just short of statistical significance. At the lowest contact pressure modelled (2 MPa), the strained polymer yielded an inconsistent layer of plastically deformed material, with a penetration depth less than 0.5  $\mu\text{m}$ . In contrast, higher contact pressure (6 MPa) produced plastic deformation in a layer almost 1  $\mu\text{m}$  thick, which grew laterally across the surface as the counterface asperity moved, creating a more continuous surface layer of deformation. The deformed region extended approximately twice as deep into the polymer bulk as compared to the lower pressure. This would suggest that increasing pressure would increase the thickness of the deformed material layer (i.e. the hypothetical ‘film’), thereby increasing ripple wavelength, according to the buckled film model.

While the computational modeling suggested that all settings across the three test parameters would produce some plastic deformation at the surface of the polymer, the extent of plastic deformation varied in both penetration depth and magnitude, as summarized in Table 2. In all of the simulations, regions of highest stress were limited to the asperities, with regions of virtually zero stress in the valleys. In spite of the early expectations that counterface roughness would play

a key role in the depth that plastic deformation occurred, it was observed that it had little effect in the computational models. This is likely due to the fact that the imported geometry of the worn polymer surface had a roughness comparable to the rough counterface ( $R_a = 0.03 \mu\text{m}$ ), so that the locations that experienced the highest stresses in any given simulation were mostly dependent on polymer asperities, rather than counterface roughness. Choosing a counterface significantly rougher than the polymer surface could result in more pronounced effects, causing more localized stresses and thicker deformation layers. Similar to roughness, temperature variation had very little effect on the magnitude or depth of plastic deformation within the simulations. While it is well known that both temperature and roughness can affect the wear rate and mechanisms [38], [39], the range of values used within this study were deliberately chosen so that all samples would maintain similar mechanisms for ripple formation. The lack of strong correlations between these factors suggests that slight variations in these parameters makes little difference in plastic deformation at the surface, and therefore little change to ripple wavelength. This is supported by the consistency in ripple wavelength seen across literature.

**Table 2:** Strain and Film Thickness Data from Finite Element Models.

Maximum principal strain				
	Low Roughness		High Roughness	
	Low Temp	High Temp	Low Temp	High Temp
Low Pressure	0.0476	0.0153	0.0211	0.0247
High Pressure	0.0765	0.0879	0.0905	0.0685

Thickness of Deformed layer ( $\mu\text{m}$ )				
	Low Roughness		High Roughness	
	Low Temp	High Temp	Low Temp	High Temp
Low Pressure	1.08	0.48	0.53	0.54
High Pressure	1.55	1.02	1.59	1.25

A clear limitation observed from the modeling results was the behavior exhibited after multiple sliding cycles. One of the primary reasons for this is that the models were designed to simulate the anticipated stress-strain behavior at the wear interface, rather than material deformation or wear. Most notably, finite element models did not demonstrate continued accumulation of strain over repeated cycles, nor did they show failure of material, despite experimental evidence that the peaks of rippled formations are drawn out until failure [30]. Instead, simulations showed that as asperities slid across each other, strain hardening of the polymer resulted in a plateau of accumulated strain, typically after only one or two passes, as shown in Figure 10. The strain that did occur was in a smooth gradient throughout the depth of the affected region. A high-fidelity simulation incorporating the large strains of a rippled topology will require a more computationally intensive

approach, likely requiring three-dimensional elements and a sophisticated material failure algorithm. However, the current results coupled with the experimental findings suggest that the rippling phenomenon is indeed directly linked to thin-film behavior of the plastically deformed layer at the wear interface.

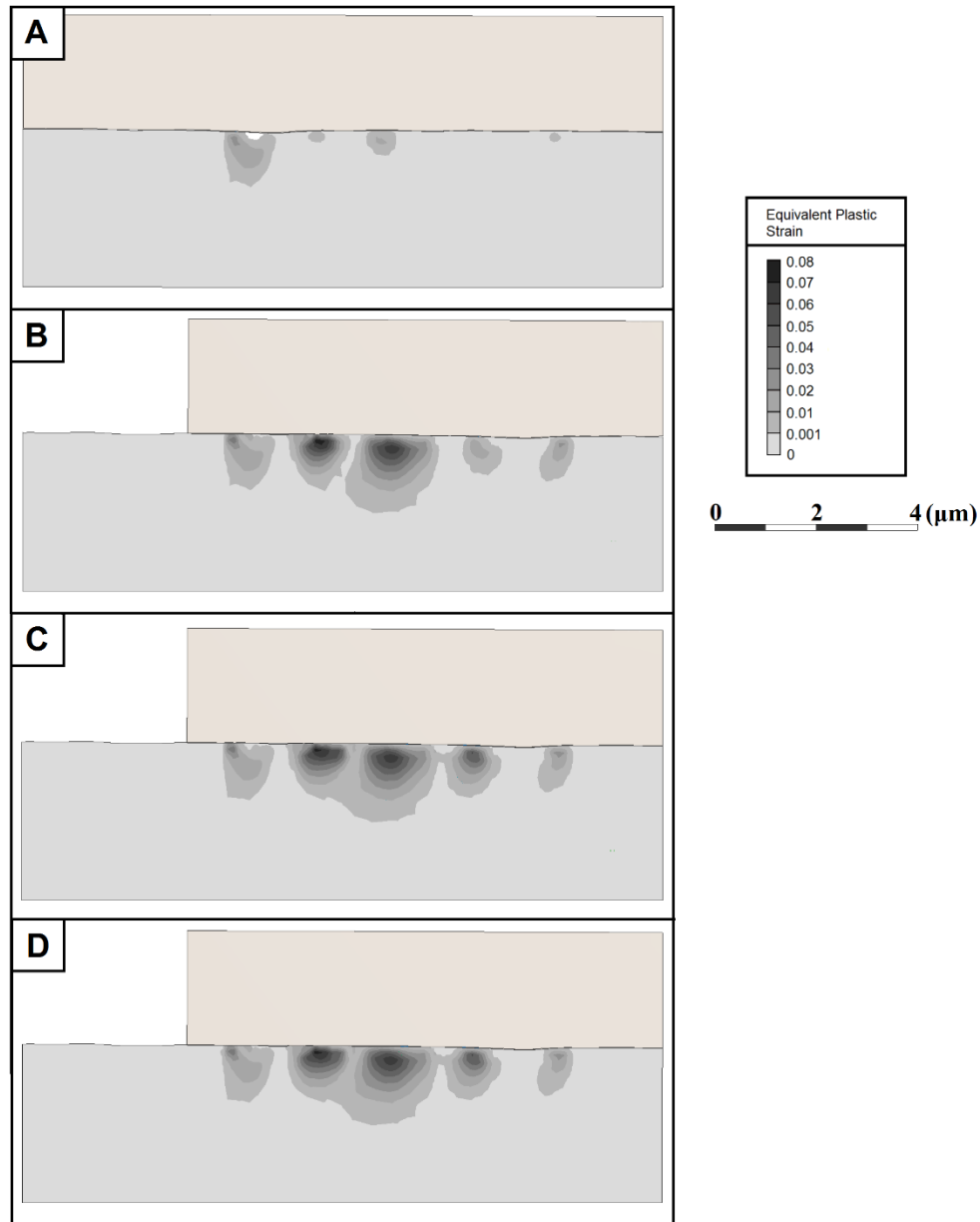


**Figure 10: Finite element results for accumulated plastic deformation between imported surface profiles for worn UHMWPE and smooth ( $R_a = 0.005 \mu\text{m}$ ) stainless steel counterface at 6MPa contact pressure. (A) At initial loading, (B) after 1 pass, (C) after 3 passes, and (D) after 7 passes. Almost no additional strain accumulates after first three passes.**

### *3.3 Study Limitations*

As with any investigation, it is necessary to discuss the limitations of the study to ensure that the results are interpreted with the appropriate context for future work. While the goal of this

investigation was to develop a better understanding of the rippling surface topology in UHMWPE as used for orthopedic bearing surfaces, care should be taken in light of the fact that this was not an *in vivo* study which mimicked all of the application conditions. Firstly, the UHMWPE material used was similar to that used in implants, however the investigators did not directly characterize microstructure or morphology of the molded pins. Furthermore, the material was not irradiated and post-stabilized as would be done with an implanted material. This means that the material studied here did not have a network of polymer crosslinks as would be found in implants. On the other hand, the rippling topology produced during the testing was very similar in appearance and size to that found in explanted polymer bearing surfaces. This could possibly be due to the fact that the surface deformation experienced in both crosslinked and non-crosslinked UHMWPE is similar in nature and thickness. Secondly, though friction is typically a very important parameter in any tribology study, it was not recorded as part of this work. The most direct explanation for this is that the test rig used was not conducive to high-precision friction measurement. However, friction also does not play a primary role in the performance of orthopedic implants because it is typically so low that it does not preclude joint articulation. Furthermore, this study showed that even in dry sliding, the rippling topology was produced similar to explanted surfaces which were immersed in synovial fluid. Clearly, friction coefficient in dry sliding is still low enough to avoid large thermal effects due to frictional heating during sliding. Thirdly, it was not possible within this study to determine whether the rippling behavior was driven primarily by intrinsic material properties or sliding conditions. However, given the repeatability of the phenomenon across a number of investigators and testing configurations, there is some indication that this behavior is more aligned with the properties of UHMWPE itself than with sliding conditions. Examination of the film buckling model corroborates this possibility because the terms of the model all relate to material properties. It is likely that testing parameters do indeed have some impact, but it will require further study to assess the relative weight of the effect of material properties versus process parameters. Fourthly, the statistical power of the study is somewhat limited by the relatively small number of samples tested. This is reflected in the non-decisive p-values reported for the factor effects. It may be appropriate in future work to use additional samples in each of the groups to further ascertain whether a multifactor interaction might be confounded with a single factor effect.

Finally, the study did not directly address previous investigations that reported a difference in orientation and size of the ripples between explanted acetabular and tibial components. In the former case, one possibility is that the ripples form perpendicular to the predominant sliding direction, while in the latter case the features appear to be aligned with sliding direction. One explanation for this apparent conflict is related to the previous argument in that the rippling may be more strongly affected by material properties and that the production of a thin deformed layer has a propensity to produce ripples regardless of sliding direction. This study illustrated that directionality of the features can vary for different regions of the pin but this was attributed to the potential for differential loading of various regions during multidirectional sliding. At this point, it is still not obvious what drives the directionality of the features, but the presence and regularity of the features did appear to be reasonably well explained by the thin film buckling model cited.

#### **4. Conclusions**

The results of this work have led to the following conclusions:

- Rippled surface geometries are consistently produced during multidirectional sliding of UHMWPE. However, this appears to start as localized patches of large wavelength ripples which eventually evolve into regularly spaced shorter wavelength features that cover large areas of the wear surface.
- Computational modeling strongly suggests that strains experienced at the wear surface are sufficient to produce plastic deformation, and thus provide conditions which can be described by an existing model of thin film buckling. Experimental results confirm plastic deformation at the surface but over a much thinner layer (on the order of 20 nm) than the computational models predict (up to 1  $\mu\text{m}$  in thickness)
- There is a clear difference in ripple spacing during the earliest stages of wear versus late-stage wear, with the latter having a shorter spacing. However, variations in pressure, counterface roughness or temperature did not appear to play a strong role in changing feature wavelength. This suggests that the ripple characteristics may be tied more closely to intrinsic material properties than sliding parameters.

## 5. References

- [1] J. H. Dumbleton, M. T. Manley, and A. A. Edidin, "A literature review of the association between wear rate and osteolysis in total hip arthroplasty," *J. Arthroplasty*, vol. 17, no. 5, pp. 649–661, 2002.
- [2] E. Oral, S. D. Christensen, A. S. Malhi, K. K. Wannomae, and O. K. Muratoglu, "Wear resistance and mechanical properties of highly cross-linked, ultrahigh-molecular weight polyethylene doped with vitamin E," *J. Arthroplasty*, vol. 21, no. 4, pp. 580–591, 2006.
- [3] O. K. Muratoglu, C. R. Bragdon, D. O. O'Connor, M. Jasty, and W. H. Harris, "A novel method of cross-linking ultra-high-molecular-weight polyethylene to improve wear, reduce oxidation, and retain mechanical properties: recipient of the 1999 HAP Paul Award," *J. Arthroplasty*, vol. 16, no. 2, pp. 149–160, 2001.
- [4] G. Lewis, "Properties of crosslinked ultra-high-molecular-weight polyethylene," *Biomaterials*, vol. 22, no. 4, pp. 371–401, 2001.
- [5] M. Jasty, H. E. Rubash, and O. Muratoglu, "Highly cross-linked polyethylene: the debate is over—in the affirmative," *J. Arthroplasty*, vol. 20, pp. 55–58, 2005.
- [6] R. Chiesa, M. C. Tanzi, S. Alfonsi, L. Paracchini, M. Moscatelli, and A. Cigada, "Enhanced wear performance of highly crosslinked UHMWPE for artificial joints," *J. Biomed. Mater. Res. Off. J. Soc. Biomater. Jpn. Soc. Biomater. Aust. Soc. Biomater. Korean Soc. Biomater.*, vol. 50, no. 3, pp. 381–387, 2000.
- [7] J. A. Savio Iii, L. M. Overcamp, and J. Black, "Size and shape of biomaterial wear debris," *Clin. Mater.*, vol. 15, no. 2, pp. 101–147, 1994.
- [8] Q. Wang, J. Liu, and S. Ge, "Study on biotribological behavior of the combined joint of CoCrMo and UHMWPE/BHA composite in a hip joint simulator," *J. Bionic Eng.*, vol. 6, no. 4, pp. 378–386, 2009.
- [9] L. Fang, Y. Leng, and P. Gao, "Processing of hydroxyapatite reinforced ultrahigh molecular weight polyethylene for biomedical applications," *Biomaterials*, vol. 26, no. 17, pp. 3471–3478, 2005.
- [10] C. H. Navarro *et al.*, "Friction and wear properties of poly (methyl methacrylate)–hydroxyapatite hybrid coating on UHMWPE substrates," *Wear*, vol. 282, pp. 76–80, 2012.

- [11] S. Ge, S. Wang, and X. Huang, "Increasing the wear resistance of UHMWPE acetabular cups by adding natural biocompatible particles," *Wear*, vol. 267, no. 5–8, pp. 770–776, 2009.
- [12] J. Tong, Y. Ma, and M. Jiang, "Effects of the wollastonite fiber modification on the sliding wear behavior of the UHMWPE composites," *Wear*, vol. 255, no. 1–6, pp. 734–741, 2003.
- [13] C. J. Schwartz, S. Bahadur, and S. K. Mallapragada, "Effect of crosslinking and Pt–Zr quasicrystal fillers on the mechanical properties and wear resistance of UHMWPE for use in artificial joints," *Wear*, vol. 263, no. 7–12, pp. 1072–1080, 2007.
- [14] Y. Chen, Y. Qi, Z. Tai, X. Yan, F. Zhu, and Q. Xue, "Preparation, mechanical properties and biocompatibility of graphene oxide/ultrahigh molecular weight polyethylene composites," *Eur. Polym. J.*, vol. 48, no. 6, pp. 1026–1033, 2012.
- [15] J. M. Dowling, J. R. Atkinson, D. Dowson, and J. Charnley, "The characteristics of acetabular cups worn in the human body," *J. Bone Joint Surg. Br.*, vol. 60, no. 3, pp. 375–382, 1978.
- [16] A. Wang, C. Stark, and J. H. Dumbleton, "Mechanistic and morphological origins of ultra-high molecular weight polyethylene wear debris in total joint replacement prostheses," *Proc. Inst. Mech. Eng. [H]*, vol. 210, no. 3, pp. 141–155, 1996.
- [17] J. Zhou and K. Komvopoulos, "Wear mechanisms of untreated and gamma irradiated ultra-high molecular weight polyethylene for total joint replacements," in *ASME/STLE 2004 International Joint Tribology Conference*, 2004, pp. 1767–1773.
- [18] K. G. Plumlee and C. J. Schwartz, "Surface layer plastic deformation as a mechanism for UHMWPE wear, and its role in debris size.," *Wear*, vol. 301, no. 1–2, pp. 257–263, 2013.
- [19] T. Asano, M. Akagi, I. C. Clarke, S. Masuda, T. Ishii, and T. Nakamura, "Dose effects of cross-linking polyethylene for total knee arthroplasty on wear performance and mechanical properties," *J. Biomed. Mater. Res. Part B Appl. Biomater. Off. J. Soc. Biomater. Jpn. Soc. Biomater. Aust. Soc. Biomater. Korean Soc. Biomater.*, vol. 83, no. 2, pp. 615–622, 2007.
- [20] C. H. da Silva and A. Sinatora, "Development of severity parameter for wear study of thermoplastics," *Wear*, vol. 263, no. 7–12, pp. 957–964, 2007.
- [21] J. Tamura *et al.*, "Micro-wear patterns on UHMWPE tibial inserts in total knee joint simulation," *J. Biomed. Mater. Res. Off. J. Soc. Biomater. Jpn. Soc. Biomater. Aust. Soc. Biomater. Korean Soc. Biomater.*, vol. 61, no. 2, pp. 218–225, 2002.
- [22] C. M. McNie, D. C. Barton, E. Ingham, J. L. Tipper, J. Fisher, and M. H. Stone, "The prediction of polyethylene wear rate and debris morphology produced by microscopic asperities on femoral heads," *J. Mater. Sci. Mater. Med.*, vol. 11, no. 3, pp. 163–174, 2000.
- [23] W. Shi, H. Dong, and T. Bell, "Tribological behaviour and microscopic wear mechanisms of UHMWPE sliding against thermal oxidation-treated Ti6Al4V," *Mater. Sci. Eng. A*, vol. 291, no. 1–2, pp. 27–36, 2000.
- [24] J. Wang, F. Yan, and Q. Xue, "Friction and wear behavior of ultra-high molecular weight polyethylene sliding against GCr15 steel and electroless Ni–P alloy coating under the lubrication of seawater," *Tribol. Lett.*, vol. 35, no. 2, pp. 85–95, 2009.
- [25] J. H. Dieterich, "Time-dependent friction and the mechanics of stick-slip," in *Rock Friction and Earthquake Prediction*, Springer, 1978, pp. 790–806.
- [26] H. Unal and A. Mimaroglu, "Friction and wear behaviour of unfilled engineering thermoplastics," *Mater. Des.*, vol. 24, no. 3, pp. 183–187, 2003.
- [27] H.-C. Kuo and M.-C. Jeng, "Dry sliding wear properties of ultra-high molecular weight polyethylene parts made by the injection molding process," *Polym.-Plast. Technol. Eng.*, vol. 50, no. 6, pp. 604–612, 2011.

- [28] A. Schallamach, "How does rubber slide?," *Rubber Chem. Technol.*, vol. 44, no. 5, pp. 1147–1158, 1971.
- [29] Q. Wang, Y. Wang, H. Wang, N. Fan, and F. Yan, "Experimental investigation on tribological behavior of several polymer materials under reciprocating sliding and fretting wear conditions," *Tribol. Int.*, vol. 104, pp. 73–82, 2016.
- [30] A. Wang, C. Stark, and J. H. Dumbleton, "Role of cyclic plastic deformation in the wear of UHMWPE acetabular cups," *J. Biomed. Mater. Res.*, vol. 29, no. 5, pp. 619–626, 1995.
- [31] J. R. Cooper, D. Dowson, and J. Fisher, "Macroscopic and microscopic wear mechanisms in ultra-high molecular weight polyethylene," *Wear*, vol. 162, pp. 378–384, 1993.
- [32] A. A. Edidin, L. Pruitt, C. W. Jewett, D. J. Crane, D. Roberts, and S. M. Kurtz, "Plasticity-induced damage layer is a precursor to wear in radiation-cross-linked UHMWPE acetabular components for total hip replacement," *J. Arthroplasty*, vol. 14, no. 5, pp. 616–627, 1999.
- [33] C. M. Stafford *et al.*, "A buckling-based metrology for measuring the elastic moduli of polymeric thin films," *Nat. Mater.*, vol. 3, no. 8, p. 545, 2004.
- [34] C. M. Stafford, B. D. Vogt, C. Harrison, D. Julthongpiput, and R. Huang, "Elastic moduli of ultrathin amorphous polymer films," *Macromolecules*, vol. 39, no. 15, pp. 5095–5099, 2006.
- [35] J. S. Bergström, C. M. Rimnac, and S. M. Kurtz, "Prediction of multiaxial mechanical behavior for conventional and highly crosslinked UHMWPE using a hybrid constitutive model," *Biomaterials*, vol. 24, no. 8, pp. 1365–1380, 2003.
- [36] A. Wang, D. C. Sun, C. Stark, Dumbleton, and JH, "Wear mechanisms of UHMWPE in total joint replacements," *Wear*, vol. 181, pp. 241–249, 1995.
- [37] M. A. Wimmer *et al.*, "A striated pattern of wear in ultrahigh-molecular-weight polyethylene components of Miller-Galante total knee arthroplasty," *J. Arthroplasty*, vol. 13, no. 1, pp. 8–16, Jan. 1998.
- [38] T. S. Barrett, G. W. Stachowiak, and A. W. Batchelor, "Effect of roughness and sliding speed on the wear and friction of ultra- high molecular weight polyethylene," *Wear*, vol. 153, no. 2, pp. 331–350, 1992.
- [39] B. Welghtman and D. Light, "The effect of the surface finish of alumina and stainless steel on the wear rate of UHMW polyethylene," *Biomaterials*, vol. 7, no. 1, pp. 20–24, 1986.